

# Near-frozen nonequilibrium state at high energy in an integrable system

Stefan G. Fischer<sup>1</sup>, Yigal Meir<sup>2</sup>, Yuval Gefen<sup>3</sup>, and Bernd Rosenow<sup>1</sup>

<sup>1</sup>*Institut für Theoretische Physik, Universität Leipzig, Brüderstrasse 16, 04103 Leipzig, Germany*

<sup>2</sup>*Department of Physics, Ben-Gurion University of the Negev, Beer-Sheva 84105, Israel*

<sup>3</sup>*Department of Condensed Matter Physics, Weizmann Institute of Science, Rehovot 76100, Israel*



(Received 6 August 2021; revised 7 July 2023; accepted 10 July 2023; published 24 August 2023)

Ergodic many-body systems are expected to reach thermal equilibrium. Here, we demonstrate that, surprisingly, high-energy electrons, which are injected into a quantum Hall edge mode with finite-range interactions, stabilize at a far-from-thermalized state over a long timescale. To detect this nonequilibrium state, one positions an energy-resolved detector downstream of the injection point. So far, nonequilibrium distributions in integrable systems were either found not to display relaxation at all, or generically relax to near-thermal asymptotic states. In stark contrast, the here-obtained many-body state comprises fast-decaying transient components, followed by a nearly frozen distribution with a peak near the injection energy.

DOI: [10.1103/PhysRevB.108.L081121](https://doi.org/10.1103/PhysRevB.108.L081121)

Many-body systems by and large tend to thermalize and display ergodicity [1–3]. This is not generally the case for integrable many-body systems. Kinematics in one dimension imposes several constraints which may undermine the ability of a many-body system to relax towards equilibrium [4–6]. The analysis of such systems is largely based on Luttinger models and generalizations thereof [7–17]. Specifically, the low-energy dynamics of the edge of quantum Hall phases is a convenient platform to test these paradigmatic concepts in a condensed matter setting [18–36]. Interestingly, for multi-channel platforms, treating interactions as short ranged still results in quasithermal states [31,32,34,37–40]. In the pure case of a chiral single-channel one-dimensional system, relaxation is not facilitated unless we consider finite-range interactions [18,21,30,41–43].

When dealing with a linear fermionic spectrum, it is well known that the relaxation of high-energy electronic excitations is suppressed due to the incompatibility of momentum and energy conservation [13–16,44]. Notwithstanding, the mere fact that the injection of particles occurs locally leads to a breaking of translational invariance and facilitates some relaxation [23,45]. In this Letter, we study this relaxation and find that it does not lead to equilibration. Furthermore, we study qualitative and robust features of this relaxation. Electrons that are locally injected at a well-defined energy interact with the channel's Fermi sea via finite-range interactions, which leads to partial energy relaxation downstream of the injection point. We predict the emergence of a rather extreme far-from-equilibrium state, in which the injected electrons remain pinned near their injection energy, giving rise to a nonmonotonous double-peak distribution. We argue that this lack of equilibration is a consequence of the weak breaking of translational invariance. Our predictions can be tested, employing local tunneling spectroscopy measurements of a chiral fermionic channel, e.g., a quantum Hall edge amenable to experimental study.

For a simplified model that features one velocity for plasmons excited from the Fermi sea and another velocity for

the injected electron, we use bosonization to compute the full nonequilibrium electron distribution as a function of the distance between the injection point and the point where electrons are detected. In order to test the result that the electron distribution exhibits a state far from thermal equilibrium which remains asymptotically stable [cf. Eq. (2) and Fig. 2], we employ a more general model of a screened interaction. The latter features a continuum of plasmon velocities. Our analysis focuses on the limit of high injection energy, in which the originally injected electron can be energetically distinguished from Fermi sea excitations. After an initial time dynamics represented by the two-velocity model, some additional relaxation takes place, which however keeps the distribution close to the injection energy, and thus far from thermal equilibrium [see Fig. 3(a)].

**General framework and results.** In order to describe the injection and detection of single electrons at specific energies in the chiral channel, we consider the model depicted in Fig. 1. A quantum dot emits an electron at energy  $\omega_i$  from a source contact into the channel at chemical potential  $\mu$  [46]. This injected electron propagates along the channel for a distance

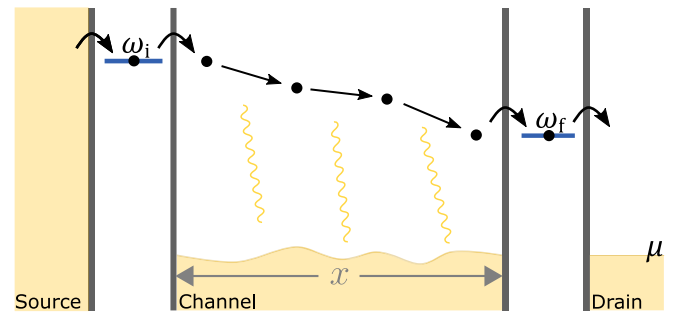


FIG. 1. An emitter quantum dot injects electrons at energy  $\omega_i$  into a chiral quantum channel, to subsequently be extracted by a detector quantum dot at energy  $\omega_f$  and distance  $x$ . Finite-ranged Coulomb interactions between electrons in the channel limit the average amount of energy transferred per interaction process.

$x$ . Subsequently, this electron itself, or electrons and holes excited during propagation (manifest through plasmons generated on top of the Fermi sea), are detected by a second quantum dot at energy  $\omega_f$ , producing a signal in the drain. The Hamiltonian for the chiral quantum channel is given by

$$H = \int dk v k \hat{c}_k^\dagger \hat{c}_k + \frac{1}{4\pi} \int dk dk' dq v_q \hat{c}_{k-q}^\dagger \hat{c}_{k'+q}^\dagger \hat{c}_{k'} \hat{c}_k. \quad (1)$$

Here,  $v$  denotes the bare velocity in the channel, the matrix element  $v_q$  constitutes the Fourier transform of the screened Coulomb interaction matrix element in real space, of strength  $v_0 = v$  and screening length  $\lambda$ . Relaxation in such channels is almost completely suppressed for injection energies  $\omega_i$  below the quotient of the highest plasmon velocity  $\bar{v}$  and the screening length  $\lambda$  [21,42,45,47]. Below this threshold, injected electrons remain energetically indistinguishable from charge carriers excited from the Fermi sea, hence relaxation is subject to Pauli blockade constraints. For pointlike interactions in real space ( $\lambda \rightarrow 0$ ), the ratio  $\bar{v}/\lambda$  diverges such that no relaxation occurs at all. In this Letter, we focus on the opposite limit  $\omega_i \gg \bar{v}/\lambda$ , and observe an inhibition of relaxation that does not rely on the aforementioned effect.

We first consider a simplified picture of a two-velocity kinematics, which features the velocity  $v$  of the electron injected at high energy and another velocity  $\bar{v} = v + v/2\pi$  for all plasmons excited from the Fermi sea. Then, the excess electron distribution  $p(\omega_f) \equiv f_{\text{Channel}}(\omega_f) - f_{\text{Drain}}(\omega_f)$  in the chiral channel featuring the electron distribution  $f_{\text{Channel}}$ , measured with respect to the ground state distribution  $f_{\text{Drain}}$  of the drain, can be obtained through bosonization. This excess distribution, which is proportional to the current in the drain, is shown in Fig. 2 for several injection energies  $\omega_i$ .

For high injection energies,  $\omega_{i_3} \gg \bar{v}/\lambda_c$  (blue curve), the injected electron can be distinguished from electrons excited from the Fermi sea (around  $\mu = 0$ ) by choosing a sufficiently high detection energy  $\omega_f$ . Within the two-velocity model,  $\lambda_c$  can be interpreted as a cutoff [42], which, similarly to the screening length  $\lambda$  above, governs the transition from the plasmonic to the fermion sector [cf. Eqs. (7) and (8) below]. The distribution of injected electrons that dissipate some of their energy (next to the delta peak for elastically transmitted electrons at  $\omega_{i_3}$  in Fig. 2) is given by

$$p_{\text{inelastic}}(x_s, \omega_{\text{if}}) \stackrel{\omega_i, \omega_f \gg \bar{v}/\lambda_c}{=} \frac{x_s^2}{x_s^2 + \lambda_c^2} \frac{\lambda_c^2}{\bar{v}^2} \omega_{\text{if}} \exp\left[-\omega_{\text{if}} \frac{\lambda_c}{\bar{v}}\right], \quad (2)$$

where  $\omega_{\text{if}} = \omega_i - \omega_f$  denotes the injected electron's energy loss. For high injection energies, the distance  $x_s = (\bar{v} - v)x/v$  corresponds to the spatial extent of the excitation arriving at the detection point (given the inherent chirality of the problem, below we refer to  $x_s$  as time); the ratio  $x_s/\lambda_c$  is the dimensionless interaction strength that controls a perturbative expansion. Remarkably, the state in Eq. (2) remains concentrated within an interval  $\bar{v}/\lambda_c$  below the injection energy, far from thermal equilibrium, even in the limit of asymptotic propagation distance  $x_s/\lambda_c \rightarrow \infty$ . For intermediate injection energies  $\omega_{i_2} \gtrsim v/\lambda_c$  (Fig. 2, yellow curve), scattering to energies in the region of energetic overlap between injected and excited electrons is reduced by Pauli blockade. At low injection energies  $\omega_{i_1} \lesssim v/\lambda_c$  (Fig. 2, green curve), Coulomb repulsion reduces the rate of electrons tunneling into the

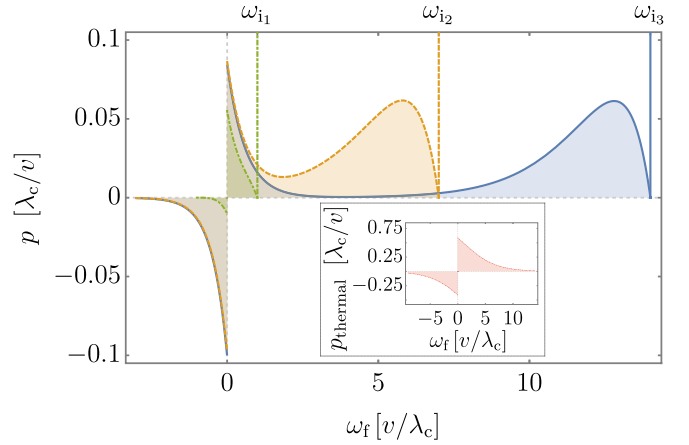


FIG. 2. The distribution  $p$  of electrons at the detection energy  $\omega_f$  with respect to the channel's ground state, after injection of an electron at energy  $\omega_i$ , is shown at a fixed distance  $x$  between injection and detection points. Here,  $p$  has been obtained from bosonization [cf. Eq. (5)] for a model that features one velocity  $v$  for the injected electron and one velocity  $\bar{v} > v$  for all plasmons in the Fermi sea [cf. Eq. (8)], at  $\bar{v} = 1.2v$  and  $x_s = 0.5\lambda_c$ , where  $\lambda_c$  corresponds to the screening length. At a high injection energy ( $\omega_{i_3} = 14v/\lambda_c$ , blue curve), the distribution of injected electrons that dissipate some of their energy (next to the delta function peak of elastically transferred electrons at  $\omega_{i_3}$ ) is completely separated from the distribution of electron-hole pairs (close to  $\mu = 0$ ). For an intermediate injection energy ( $\omega_{i_2} = 7v/\lambda_c$ , yellow curve), scattering to energies in the region of energetic overlap between injected and excited electrons is suppressed by Pauli blockade. At a low injection energy ( $\omega_{i_1} = v/\lambda_c$ , green curve), Coulomb repulsion reduces the rate of electrons tunneling into the channel (zero-bias anomaly [37]), and Pauli blockade further reduces relaxation.

channel (zero-bias anomaly [37]), and Pauli blockade further reduces relaxation.

Taking into account screened interactions in the system generates a continuum of plasmon velocities ranging from  $v$  to  $\bar{v}$ . This takes us beyond the two-velocity picture. A full resummation of the high-energy electron-plasmon perturbation theory, and numerical evaluation of the thus-obtained electron distribution for the aforementioned type of interaction, constitutes our main result. This numerically obtained electron distribution is displayed in Fig. 3(a), for several values of  $x_s$ .

Initially, the dynamics of the distribution [ $x_s = 0$  to blue triangle in Fig. 3(b)] resembles the dynamics obtained from the model in which all plasmons share the same velocity  $\bar{v}$  [compare the solid blue curve at  $x_s = 2.2\lambda$  in Fig. 3(a), and the solid blue curve in Fig. 2, next to  $\omega_{i_3}$ ]. In contrast to the two-velocity model, this buildup period is here followed by a phase of rapid decay [blue triangle to green circle in Fig. 3(b)]. Remarkably, after this phase of decay, the center as well as the maximum of the distribution decay only very slowly [green circle to red asterisk in Fig. 3(b)] towards the Fermi level at  $\omega_f = 0$ . Dissipation of the injected electron's energy is inhibited, such that the distribution remains metastable close to the injection energy  $\omega_i$ , and thus far from thermal, on a length scale that far exceeds the screening length.

*Bosonization approach.* In the following, the theoretical background to obtain the above-described results is laid out.

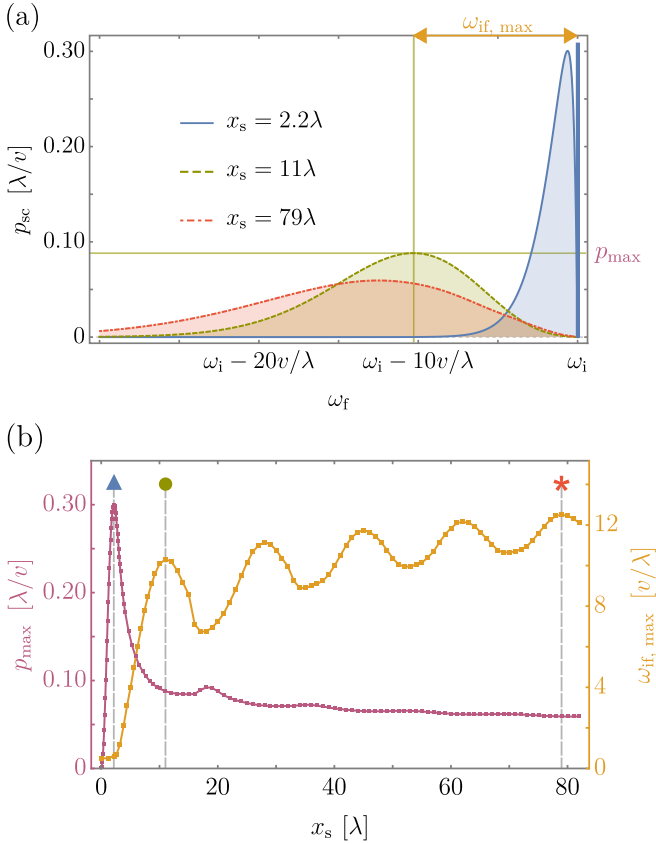


FIG. 3. (a) Distribution  $p_{sc}$  of high-energy injected electrons that underwent relaxation [cf. Eq. (9)], as a function of detection energy  $\omega_f$ , for several values of  $x_s$ . Here, this distribution has been obtained for the screened interaction (6), which gives rise to a continuum of plasmon velocities in the Fermi sea. The energy loss  $\omega_{if,max}$  (yellow arrows) at the maximum of the distribution  $p_{max}$  (horizontal green line) is indicated for  $x_s = 11\lambda$ , after the distribution underwent buildup and a short period of rapid decay (green curve). Following this period,  $p_{sc}$  varies only slowly, and remains far from thermal equilibrium. The vertical blue line at the injection energy  $\omega_i$  indicates elastic transfer (no energy loss). The probability of such transfer at  $x_s = 2.2\lambda$  ( $P_{elastic} \approx 0.31$ ) significantly exceeds the respective values at  $x_s = 11\lambda$  ( $P_{elastic} \approx 9.3 \times 10^{-6}$ ) and  $x_s = 79\lambda$  ( $P_{elastic} \approx 4.0 \times 10^{-7}$ ); the latter are not indicated. (b) Energy loss  $\omega_{if,max}$  (yellow) and peak height  $p_{max}$  (purple) of the distribution  $p_{sc}$ , as a function of  $x_s$  [markers indicate  $x_s$  values corresponding to distributions in (a)]. After an initial buildup period ( $x_s = 0$  to blue triangle), followed by a rapid decay (blue triangle to green circle), the electron distribution develops a metastable profile. The distribution as a function of  $x_s$  then varies only slowly on the scale of the screening length (cf. green circle to red asterisk), and does not display efficient decay towards the Fermi level located at  $\omega_f = 0$ .

Linearity of the fermionic dispersion relation in the first term of Eq. (1) allows to obtain the greater (+) and lesser (−) Green's functions of the channel via bosonization [30,41–43],

$$G^\pm(x, t) = G_0^\pm(x, t)e^{S^\pm(x, t)}. \quad (3)$$

Here, the noninteracting Green's function  $G_0^\pm(x, t) = 1/2\pi(x - vt \pm i\epsilon)$  has been separated from the part that

describes interactions via the exponent [42]

$$S^\pm(x, t) = \int_0^\infty \frac{dq}{q} (e^{\mp i(\omega_q t - qx)} - e^{\mp i(v_q t - qx)}). \quad (4)$$

The bosonic dispersion relation  $\omega_q = vq(1 + v_q/2\pi v)$  determines the velocities of the collective plasmon modes.

Given that tunneling to and from emitter and detector quantum dots is weak, the current out of and into the drain is proportional to the distribution of electrons at propagation length  $x$  [48] and energy  $\omega_f$  with respect to the ground state of the channel, provided that an electron tunnels into this channel at  $\omega_i$ . The general expression for this distribution is given by [49–51]

$$\begin{aligned} p(x, \omega_i, \omega_f) &= \frac{v^2}{2\pi} \int_{-\infty}^{+\infty} dt_0 \int_{-\infty}^{+\infty} dt_1 \int_{-\infty}^{+\infty} dt_2 e^{i\omega_f t_0} e^{-i\omega_i(t_1 - t_2)} \\ &\times G^-(0, t_1 - t_2) G^\alpha(0, -t_0) [\Pi^{++}(x, 0, t_0, t_1, t_2) \\ &- \Pi^{--}(x, 0, t_0, t_1, t_2)], \end{aligned} \quad (5)$$

where  $\alpha$  denotes the lesser component (−) for  $\omega_f < 0$  (below the Fermi level), and the greater component (+) for  $\omega_f > 0$  (above the Fermi level), and  $\Pi^{\beta\gamma}(x, t_0, t_1, t_2, t_3) = G^\beta(x, t_0 - t_3) G^\gamma(x, t_1 - t_2) / G^\beta(x, t_1 - t_3) G^\gamma(x, t_0 - t_2)$ .

For interactions that decay exponentially in momentum space,

$$v_q^{(exp)} = v \exp(-\lambda|q|), \quad (6)$$

we perform an order-by-order integration of Eq. (4) in an expansion in powers of  $v/2\pi v$ , which leads to

$$S^{(exp)\pm}(x, t) = \sum_{k=1}^{\infty} \frac{1}{k} \left[ \frac{\frac{v}{2\pi} t}{x - vt \pm i\lambda k} \right]^k. \quad (7)$$

Within the two-velocity approximation, one replaces  $\lambda k$  by  $\lambda_c$  (for all  $k$ ) and obtains (cf. Supplemental Material [52])

$$G_{v-\bar{v} \text{ model}}^\pm(x, t) = \frac{1}{2\pi} \frac{1}{x - vt \pm i\epsilon} \frac{x - vt \pm i\lambda_c}{x - \bar{v}t \pm i\lambda_c} \quad (8)$$

(cf. Refs. [21,42]), which display poles determined by the velocity  $v$  of high-energy electrons (which corresponds to the slope of  $\omega_q$  for large  $q \gg 1/\lambda$ ) and the velocity of low-energy plasmons  $\bar{v}$  (given by the slope of  $\omega_q$  at  $q = 0$ ).

Employing the thus-obtained Green's functions in Eq. (8), we can evaluate the relaxation distribution in Eq. (5) analytically. Above the Fermi sea,  $\omega_f > 0$ , the electron distribution of Eq. (5) features two contributions,  $p(\omega_f > 0) = P_{elastic}\delta(\omega_i - \omega_f) + p_{inelastic}\theta(\omega_i - \omega_f)$ . The first contribution,  $P_{elastic}$ , has been investigated in detail [42,43], and describes the weight of the delta peaks located at the injection energies  $\omega_i$  in Fig. 2. The second contribution to the electron current,  $p_{inelastic}$  (for explicit expressions see Supplemental Material [52]), is composed of three parts: the distribution in Eq. (2), that corresponds to the originally injected electron entering the detector at an energy other than the injection energy  $\omega_i$ , the distribution  $p_{exc}^e$  of electrons excited from the Fermi sea entering the detector, as well as interference terms (cf. the discussion based on perturbation theory [45] which, in contrast to present results, diverges for  $x_s \gg \lambda$ ).

Below the Fermi sea,  $\omega_f < 0$ , we find  $p(\omega_f < 0) = p_{\text{exc}}^h \theta(\omega_i + \omega_f) + p_{\text{int}}^h \theta(\omega_i + \omega_f)$  which entails a contribution  $p_{\text{exc}}^h$  of holes left behind by excited electrons  $p_{\text{exc}}^e$ , as well as interference terms  $p_{\text{int}}^h$  (see Supplemental Material [52]). The full electron distribution obtained from Eq. (5) is displayed in Fig. 2, for several values of the injection energy  $\omega_i$ . In the limit of high injection energies,  $\omega_i \gg \bar{v}/\lambda_c$  ( $\omega_{i3} = 14v/\lambda_c$ , solid blue), injected and excited electrons are energetically well separated, and all above-mentioned interference terms vanish. For intermediate injection energies ( $\omega_{i2} = 7v/\lambda_c$ , dashed yellow), scattering to energies in the region of energetic overlap of injected and excited electrons is suppressed by Pauli blockade. At low injection energies ( $\omega_{i1} = v/\lambda_c$ , dotted-dashed green), Coulomb repulsion reduces the rate of electrons tunneling into the channel (zero-bias anomaly [37]), and Pauli blockade further reduces relaxation.

*Semiclassical approach.* To evaluate the distribution of injected electrons for arbitrary screened interactions  $v_q$ , which allows for a continuum of plasmon velocities, we separate the contribution of injected electrons that are detected close to the injection energy from charge carriers excited from the Fermi sea. Within this semiclassical picture, valid at high injection energies (cf. Refs. [42–44] and Supplemental Material [52]), we provide a full resummation of a perturbation expansion that treats the injected electron as distinguishable from bosonized plasmons in the Fermi sea, and fixes the injected electrons transition time at  $t = x/v$ . The approach generates the expression (cf. Supplemental Material [52])

$$p_{\text{sc}}(x, \omega_{\text{if}}) = \int_{-\infty}^{\infty} \frac{dt}{2\pi} e^{i\omega_{\text{if}}t} \times \exp \left\{ \int_0^{\infty} \frac{dq}{q} 4 \sin^2 \left[ \frac{qx}{2} \frac{v_q}{2\pi v} \right] (e^{-i\omega_q t} - 1) \right\}, \quad (9)$$

in which the second term in the exponential corresponds to the contribution of elastic transport in which no plasmons are excited, and the first term in Eq. (9) in the exponential contains the information about relaxation via excitation of any finite number of plasmons. The squared sine factor in Eq. (9) precisely results from the mismatch of the dispersion of the high-energy electron at energy  $vq$  and the dispersion of low-energy plasmons at energy  $\omega_q$ , and the argument of this factor encodes energy-time uncertainty between this mismatch  $\Delta\omega = \omega_q - vq$  and the transit time of the high-energy electron  $\Delta t = x/v$ . Thus, longer  $\Delta t$  favor larger momentum transfer, for which the discrepancy  $\Delta\omega$  becomes smaller. At the same time, large momentum transfer is hampered by the finite-ranged nature of interactions which causes a cutoff in momentum space, such that the observed inhibition of relaxation likely emerges as a result of these two competing mechanisms.

To test the validity of the high injection energy expression in Eq. (9), we insert Eq. (8), which features one velocity  $\bar{v}$  for all excited plasmons in the Fermi sea, into Eq. (9), written in terms of Green's functions (see Supplemental Material [52]). This directly produces Eq. (2), which had initially been obtained by evaluation of the full distribution given by Eq. (5), followed by the limit  $\omega_i \gg \frac{\bar{v}}{\lambda}$ ,  $\omega_{\text{if}}$ . For exponentially decaying

interactions, Eq. (6), we evaluate Eq. (9) numerically after taking a scaling limit in which  $x/\lambda \rightarrow \infty$  and  $v/2\pi v \rightarrow 0$ , while the product  $x_s/\lambda$  of these two quantities is kept constant [53] (cf. Supplemental Material [52]).

*Discussion.* Results of this numerical evaluation are displayed in Fig. 3. Figure 3(a) shows the energy distribution of the arriving particles  $p_{\text{sc}}$ , for several values of effective interaction strength  $x_s/\lambda$ . Initially (short times,  $x_s = 2.2\lambda$ , see the blue curve), the distribution is very similar to the prediction of the two-velocity model. At intermediate times ( $x_s = 11\lambda$ , green curve) one observes rapid decay, while for longer timescales ( $x_s = 79\lambda$ , red curve) the decay is very slow. The slow decay of the distribution is made further apparent in Fig. 3(b), which shows the maximum  $p_{\text{max}}$  of the distribution as well as the energy loss  $\omega_{\text{if, max}}$  at this maximum, as a function of time  $x_s$ . The quantities  $\omega_{\text{if, max}}$  and  $p_{\text{max}}$ , as well as the entire distribution display oscillatory behavior, which they share with the magnitude of the elastic contribution [42,43,52]. The frequency of this oscillation corresponds to the maximum of the Galileo transformed bosonic spectrum  $\omega_q - vq$  [54]. The decay of  $p_{\text{sc}}$  as a function of  $x_s/\lambda$  is markedly slow;  $\omega_{\text{if, max}}$  and  $p_{\text{max}}$  can be fitted to weak power laws  $\omega_{\text{if, max}} \sim (x_s/\lambda)^{0.101 \pm 0.004}$  and  $p_{\text{max}} \sim (x_s/\lambda)^{-0.202 \pm 0.006}$ . This fit was performed at those  $x_s/\lambda$  at which  $p_{\text{sc}}^{(0)}$  displays the first five local minima. Note though that asymptotic saturation cannot be excluded.

We conclude by noting that GaAs and graphene are candidate materials for the observation of the above-described metastable electronic distribution. At 10 T, the energy gap between the zeroth and first Landau levels in GaAs is about 17 meV [55], and 115 meV in graphene [56]. The unit of energy  $\hbar\bar{v}/\lambda$  for our results depicted in Fig. 3, at an estimated screening length of 0.5  $\mu\text{m}$ , amounts to 0.1 meV in GaAs and 1 meV in graphene. For both materials, the gap thus accommodates the entire energy range displayed in Fig. 3 by a wide margin. Quantum dot spectroscopy experiments have already been carried out in GaAs at high injection energies [23,24], and isolation of a single channel from a multichannel system has been experimentally realized [24,35,57]. In graphene, precise control of transport has recently been demonstrated in Fabry-Pérot interferometers [58,59].

In summary, we have investigated the relaxation of electrons injected into a one-dimensional chiral channel, which interact with charge carriers in the channel via finite-ranged interactions. For a simplified model that features one velocity of incoming electrons and one velocity for plasmons in the Fermi sea, we found a stable highly nonthermal state, concentrated close to the energy of injected electrons. For a more realistic model that features a continuum of plasmon velocities, we predict a state that remains nearly frozen close to high injection energies, far from thermal equilibrium.

*Acknowledgments.* We would like to acknowledge useful discussions with Jinhong Park, Kyrylo Snizhko, and Felix Puster. Y.G. and B.R. acknowledge support by DFG RO 2247/11-1. Y.M. acknowledges support from ISF Grant No. 359/20. Y.G. further acknowledges support by the Helmholtz International Fellow Award, CRC 183 (Project No. C01), and the German-Israeli Foundation Grant No. I-1505-303.10/2019. Y.G. and S.G.F. acknowledge support by the Minerva foundation.



- [1] A. Polkovnikov, K. Sengupta, A. Silva, and M. Vengalattore, *Rev. Mod. Phys.* **83**, 863 (2011).
- [2] J. Eisert, M. Friesdorf, and C. Gogolin, *Nat. Phys.* **11**, 124 (2015).
- [3] C. Gogolin and J. Eisert, *Rep. Prog. Phys.* **79**, 056001 (2016).
- [4] M. Rigol, V. Dunjko, V. Yurovsky, and M. Olshanii, *Phys. Rev. Lett.* **98**, 050405 (2007).
- [5] T. Kinoshita, T. Wenger, and D. S. Weiss, *Nature (London)* **440**, 900 (2006).
- [6] S. Hofferberth, I. Lesanovsky, B. Fischer, T. Schumm, and J. Schmiedmayer, *Nature (London)* **449**, 324 (2007).
- [7] J. Sólyom, *Adv. Phys.* **28**, 201 (1979).
- [8] E. Miranda, *Braz. J. Phys.* **33**, 3 (2003).
- [9] J. von Delft and H. Schoeller, *Ann. Phys.* **510**, 225 (1998).
- [10] I. V. Lerner, V. I. Yudson, and I. V. Yurkevich, *Phys. Rev. Lett.* **100**, 256805 (2008).
- [11] A. Calzona, F. M. Gambetta, M. Carrega, F. Cavaliere, and M. Sassetti, *Phys. Rev. B* **95**, 085101 (2017).
- [12] A. Štrkalj, M. S. Ferguson, T. M. R. Wolf, I. Levkivskiy, and O. Zilberberg, *Phys. Rev. Lett.* **122**, 126802 (2019).
- [13] V. V. Deshpande, M. Bockrath, L. I. Glazman, and A. Yacoby, *Nature (London)* **464**, 209 (2010).
- [14] G. Barak, H. Steinberg, L. N. Pfeiffer, K. W. West, L. Glazman, F. Von Oppen, and A. Yacoby, *Nat. Phys.* **6**, 489 (2010).
- [15] E. G. Idrisov and T. L. Schmidt, *Phys. Rev. B* **100**, 165404 (2019).
- [16] A. Imambekov, T. L. Schmidt, and L. I. Glazman, *Rev. Mod. Phys.* **84**, 1253 (2012).
- [17] T. Giamarchi, *Quantum Physics in One Dimension* (Oxford University Press, Oxford, UK, 2004).
- [18] P. Degiovanni, C. Grenier, and G. Fève, *Phys. Rev. B* **80**, 241307(R) (2009).
- [19] D. Ferraro, B. Roussel, C. Cabart, E. Thibierge, G. Fève, C. Grenier, and P. Degiovanni, *Phys. Rev. Lett.* **113**, 166403 (2014).
- [20] M. Acciai, A. Calzona, G. Dolcetto, T. L. Schmidt, and M. Sassetti, *Phys. Rev. B* **96**, 075144 (2017).
- [21] C. Cabart, B. Roussel, G. Fève, and P. Degiovanni, *Phys. Rev. B* **98**, 155302 (2018).
- [22] A. S. Goremykina and E. V. Sukhorukov, *Phys. Rev. B* **97**, 115418 (2018).
- [23] T. Krähenmann, S. G. Fischer, M. Rössli, T. Ihn, C. Reichl, W. Wegscheider, K. Ensslin, Y. Gefen, and Y. Meir, *Nat. Commun.* **10**, 3915 (2019).
- [24] R. H. Rodriguez, F. D. Parmentier, D. Ferraro, P. Roulleau, U. Gennser, A. Cavanna, M. Sassetti, F. Portier, D. Mailly, and P. Roche, *Nat. Commun.* **11**, 2426 (2019).
- [25] G. Rebora, D. Ferraro, R. H. Rodriguez, F. D. Parmentier, P. Roche, and M. Sassetti, *Entropy* **23**, 138 (2021).
- [26] H. le Sueur, C. Altimiras, U. Gennser, A. Cavanna, D. Mailly, and F. Pierre, *Phys. Rev. Lett.* **105**, 056803 (2010).
- [27] P. Degiovanni, C. Grenier, G. Fève, C. Altimiras, H. le Sueur, and F. Pierre, *Phys. Rev. B* **81**, 121302(R) (2010).
- [28] C. Altimiras, H. Le Sueur, U. Gennser, A. Cavanna, D. Mailly, and F. Pierre, *Nat. Phys.* **6**, 34 (2010).
- [29] A. M. Lunde, S. E. Nigg, and M. Büttiker, *Phys. Rev. B* **81**, 041311(R) (2010).
- [30] D. L. Kovrizhin and J. T. Chalker, *Phys. Rev. B* **84**, 085105 (2011).
- [31] I. P. Levkivskiy and E. V. Sukhorukov, *Phys. Rev. B* **85**, 075309 (2012).
- [32] M. Millettari and B. Rosenow, *Phys. Rev. Lett.* **111**, 136807 (2013).
- [33] A. O. Slobodeniuk, E. G. Idrisov, and E. V. Sukhorukov, *Phys. Rev. B* **93**, 035421 (2016).
- [34] A. Schneider, M. Millettari, and B. Rosenow, *SciPost Phys.* **2**, 007 (2017).
- [35] H. Duprez, E. Sivre, A. Anthore, A. Aassime, A. Cavanna, A. Ouerghi, U. Gennser, and F. Pierre, *Phys. Rev. X* **9**, 021030 (2019).
- [36] A. Borin and E. Sukhorukov, *Phys. Rev. B* **99**, 085430 (2019).
- [37] D. B. Gutman, Y. Gefen, and A. D. Mirlin, *Phys. Rev. Lett.* **101**, 126802 (2008).
- [38] A. Iucci and M. A. Cazalilla, *Phys. Rev. A* **80**, 063619 (2009).
- [39] H. Inoue, A. Grivnin, N. Ofek, I. Neder, M. Heiblum, V. Umansky, and D. Mahalu, *Phys. Rev. Lett.* **112**, 166801 (2014).
- [40] K. Itoh, R. Nakazawa, T. Ota, M. Hashisaka, K. Muraki, and T. Fujisawa, *Phys. Rev. Lett.* **120**, 197701 (2018).
- [41] J. T. Chalker, Y. Gefen, and M. Y. Veillette, *Phys. Rev. B* **76**, 085320 (2007).
- [42] C. Neuenhahn and F. Marquardt, *New J. Phys.* **10**, 115018 (2008).
- [43] C. Neuenhahn and F. Marquardt, *Phys. Rev. Lett.* **102**, 046806 (2009).
- [44] M. Heyl, S. Kehrein, F. Marquardt, and C. Neuenhahn, *Phys. Rev. B* **82**, 033409 (2010).
- [45] S. G. Fischer, J. Park, Y. Meir, and Y. Gefen, *Phys. Rev. B* **100**, 195411 (2019).
- [46] The chemical potential  $\mu$  defines the reference energy which is set to zero throughout the Letter.
- [47] T. Karzig, *Low dimensional electron systems out of equilibrium*, Dissertation, Freie Universität Berlin, 2012.
- [48] The propagation length  $x$  corresponds to the separation of emitter and detector quantum dots along the edge channel that extends from negative to positive infinity.
- [49] C. L. Kane and M. P. A. Fisher, *Phys. Rev. B* **67**, 045307 (2003).
- [50] S. Takei, M. Millettari, and B. Rosenow, *Phys. Rev. B* **82**, 041306(R) (2010).
- [51] C. Han, J. Park, Y. Gefen, and H.-S. Sim, *Nat. Commun.* **7**, 11131 (2016).
- [52] See Supplemental Material at <http://link.aps.org/supplemental/10.1103/PhysRevB.108.L081121> for additional analysis and results characterizing the energy relaxation of high energy electrons injected into a single chiral channel, interacting with the Fermi sea via a finite range interaction.
- [53] For, e.g., the distribution in Eq. (2) in dimensionless form,  $\bar{v} p_{\text{inelastic}}/\lambda$ , this approximation corresponds to  $\bar{v} \rightarrow v$ , which only lowers the energy scale  $\bar{v}/\lambda$  of the function's dependence on  $\omega_{\text{if}}$ . In Eq. (9), the approximation corresponds to  $\omega_q \rightarrow vq$  in the second exponential term.
- [54] For  $v_{q, \text{exp}}$  (6),  $\omega_{q, \text{max}}^G = v/2\pi\lambda e$ .
- [55] C. W. J. Beenakker and H. van Houten, *Solid State Phys.* **44**, 1 (1991).
- [56] Y. J. Song, A. F. Otte, Y. Kuk, Y. Hu, D. B. Torrance, P. N. First, W. A. De Heer, H. Min, S. Adam, M. D. Stiles, A. H. MacDonald, and J. A. Stroscio, *Nature (London)* **467**, 185 (2010).

- [57] C. Altimiras, H. le Sueur, U. Gennser, A. Cavanna, D. Mailly, and F. Pierre, [Phys. Rev. Lett.](#) **105**, 226804 (2010).
- [58] C. Déprez, L. Veyrat, H. Vignaud, G. Nayak, K. Watanabe, T. Taniguchi, F. Gay, H. Sellier, and B. Sacépé, [Nat. Nanotechnol.](#) **16**, 555 (2021).
- [59] Y. Ronen, T. Werkmeister, D. Haie Najafabadi, A. T. Pierce, L. E. Anderson, Y. J. Shin, S. Y. Lee, Y. H. Lee, B. Johnson, K. Watanabe, T. Taniguchi, A. Yacoby, and P. Kim, [Nat. Nanotechnol.](#) **16**, 563 (2021).